Critical slip and time dependence in sea ice friction

Ben Lishman[+], Institute for Risk and Disaster Reduction, University College London
Peter R Sammonds, Institute for Risk and Disaster Reduction, University College London
Danny L Feltham, Centre for Polar Observation and Monitoring, University College London

Abstract

Recent research into sea ice friction has focussed on ways to provide a model which maintains much of the clarity and simplicity of Amonton's law, yet also accounts for memory effects. One promising avenue of research has been to adapt the rate- and state- dependent models which are prevalent in rock friction. In such models it is assumed that there is some fixed critical slip displacement, which is effectively a measure of the displacement over which memory effects might be considered important. Here we show experimentally that a fixed critical slip displacement is not a valid assumption in ice friction, whereas a constant critical slip time appears to hold across a range of parameters and scales. As a simple rule of thumb, memory effects persist to a significant level for 10s. We then discuss the implications of this finding for modelling sea ice friction and for our understanding of friction in general.

Keywords: ice, friction, critical slip

Highlights

- Sea ice friction shows memory, which decays over a fixed time.
- A rate-and-state model can be used to quantify this memory.
- Model predictions agree well with experimentally measured dynamic friction.

+: Corresponding author: e: b.lishman@ucl.ac.uk, t: +44 203108 1104, f: +44 207679 2433
Ben Lishman, Institute for Risk and Disaster Reduction, University College London, Gower Street, London, WC1E6BT, United Kingdom.

Sea ice friction and memory effects

The behaviour of sea ice ensembles is of scientific and engineering interest on a range of scales, from determining local forces on an ice-moored structure to predicting whole-Arctic behaviour in climate models. Sea ice deformation is controlled by friction, through ridging, rafting, and in-plane sliding. Dry friction, on the macroscopic scale, is well understood by Amonton's law (that the ratio of shear to normal forces on a sliding interface is a constant, μ). Ice friction, in contrast, involves processes of melting and freezing, and associated lubrication and adhesion, and is hence somewhat more complicated. One key understanding is that when melting and freezing occur, friction can only be predicted if we know the state of the sliding interface, and hence memory effects must be included in any model.

There are two different approaches to this challenge, and progress has been made in both. The first is to work towards a better understanding of the detailed thermodynamics and micromechanics of ice friction. Work on lubrication models of ice friction has built on the foundation provided by Oksanen and Keinonen (1982); the effects of freezing have been summarised by Maeno and Arakawa (2004); the micromechanics of asperity contacts are considered by e.g. Hatton et al., 2009. The second possibility is to work on empirical adaptations of Amonton's law to incorporate memory effects (see e.g. Lishman et al., 2009, 2011; Fortt and Schulson, 2009). It seems reasonable to believe that the two approaches are mutually compatible, and might combine to provide a clearer picture of ice friction.

One empirical adaptation of Amonton's law which has gained significant traction in the rock mechanics literature is a rate and state friction model. Such a model accounts for two properties of friction which are frequently empirically observed:

1) Friction depends on the rate at which surfaces slide past each other, and
2) The state of the sliding surface affects the friction coefficient, and is itself affected by frictional sliding.

Friction in such models is assumed to be composed of a constant value, a rate-dependent term, and one or more state variables (see Ruina (1983) for discussion). The simplest rate and state model has the form:

$$\mu = \mu_0 + \theta + A \ln \frac{V}{V^*} \tag{1a}$$

$$\frac{d\theta}{dt} = -\frac{V}{L} \left(\theta + B \ln \frac{V}{V^*}\right) \tag{1b}$$

where μ is the time-dependent effective friction coefficient, V is the slip rate, V* is a characteristic slip rate, and θ is the state variable, which affects the overall friction coefficient (equation 1a) and varies with sliding (equation 1b). A, B, and μ_0 are empirically determined parameters of the model. In this work, however, we wish to focus on L, the critical slip displacement. Ruina (1983) states that one basic feature of a system which fits a rate and state model is that "the decay of stress value after [a] step change in slip rate has characteristic length that [is] independent of slip rate". Ruina notes that this feature "appears to be common to the limited recent observations" in rock mechanics. Both Lishman et al., 2009, and Fortt and Schulson, 2009, have gone on to make the assumption that a critical slip displacement is also a characteristic of ice friction.

The critical slip displacement is best understood graphically from figure 1. The upper graph shows an instantaneous change in slip rate across a sliding interface, while the lower part shows the typical frictional response for such a change. Qualitatively, such a response has been shown to occur in ice (Fortt and Schulson, 2009). Under steady sliding at initial slip rate V_1, friction is steady at some constant value μ_1^{ss}. On acceleration, friction instantaneously increases to some value μ_{peak}, and then gradually decays to some new steady state value μ_2^{ss}. The critical slip displacement, L, is defined as the distance over which friction decays from μ_{peak} to $[e^{-1}(\mu_{peak} - \mu_2^{ss}) + \mu_2^{ss}]$ (hereon abbreviated to μ_{cs}), and is shown as such on figure 1.

In this work we wish to better understand the critical slip of sea ice, and so we are particularly interested in the scaling of the frictional decay from μ_{peak} to μ_2^{ss}, and this region of interest (R.O.I.) is marked with a dot-dashed line: the R.O.I. is what will be shown in later experimental plots. Further, since we are interested in the scaling of the decay, we normalize for μ_{peak} and μ_2^{ss}. Experimental plots will therefore be shown as normalized friction μ_n:

$$\mu_n = \frac{\mu - \mu_2^{SS}}{\mu_{peak} - \mu_2^{SS}} \tag{2}$$

to allow straightforward comparison across results with varying μ_{peak} and μ_2^{ss}.

The scaling of slip in sea ice

We investigate the critical slip of sea ice in a series of laboratory experiments. Sea ice is grown in the UCL Rock and Ice Physics cold room facilities using carefully insulated cylinders to ensure a vertically oriented columnar ice structure comparable to that found in nature, with typical grain dimensions 10mm in the horizontal (x-y) plane and 50mm in the vertical (z) direction (see Lishman et al., 2011 for further details and thin sections). The ice is then cut to approximate shape using a bandsaw and milled to 100µm precision. Figure 2 shows the experimental setup, with three ice blocks (300×100×100mm) in a double shear configuration. The sliding faces are in the x-z plane, analogous to the sliding of floating ice floes in nature. One key distinction between experiment and nature is that the experiment occurs out of the saline water, and so to minimise brine drainage we conduct all experiments within 4 hours of removing the ice from water. Table 1 gives further details of the ice properties. Normal load is provided by a hydraulic load frame, while shear load is provided by a hydraulic actuator. The entire experiment occurs within an environmental chamber in which temperature can be controlled. All loads and displacements are monitored at sub-100ms intervals using externally calibrated load cells and displacement transducers.

Twelve experiments were run with this experimental setup and various environmental conditions, and the relevant conditions for each experiment are given in table 2. The same ice blocks were used throughout. In each experiment the central block is moved 30mm, under normal load, to ensure a repeatable sliding surface. Motion is then stopped for a given hold time (listed for each experiment in table 2): this gives $V_1=0$. Motion is then instantaneously resumed at some slip rate V_2, again given for each experiment in table 2. This leads to a frictional decay profile similar to that shown in figure 1. Figure 3a shows a typical actuator velocity profile for an experiment with $V_2=1\text{mms}^{-1}$, and we note that the laboratory actuator acceleration is around 1mms^{-2}. Normalised frictional decays are shown for all experiments with $V_2=0.1\text{mms}^{-1}$ in figure 3b, and for all experiments with $V_2=1\text{mms}^{-1}$ in figure 3c. For each experiment μ_{peak} and μ_2^{ss} are given in table 2 so that normalised friction μ_n can be reconverted into absolute friction. The contrast between figure 3b and figure 3c is clear. Although the critical slip in figure 3b is somewhat obscured by secondary stick-slip behaviour (cf. Fortt and Schulson, 2009), the decay from peak friction (1 on the normalised scale) to steady state friction clearly occurs within the first 1mm of slip. In contrast the equivalent decay in figure 3b occurs over around 10mm of slip. This holds true independent of hold time, temperature or side load.

However, it seems plausible that this difference in critical slip displacement is related to the stick-slip behaviour which occurs at low speeds. To test this hypothesis we compare our results from the UCL experiments to a series of ice tank experiments undertaken at the HSVA facility in Hamburg, Germany in the summer of 2008. In these experiments the sliding interfaces are 2m long, and the slip rate is $16mms^{-1}$. The normal load is provided by pneumatic load frames and the shear load by a mechanical pusher carriage. Full experimental details can be found in Lishman et al, 2009. Results from these experiments, directly comparable to those of experiments 1-12, are shown in figure 3d. Here we see that at the higher slip rate the critical slip displacement increases to roughly 120mm.

The results from these experiments, across different scales, strongly suggest that the critical slip displacement of ice is not a constant. Moreover, the apparently linear increase of critical slip displacement with slip rate suggests that there may be a relevant critical slip time which governs all the observed slip decays. A simple exponential decay with time is overlaid on each of the plots:

$$\mu_n = e^{-0.32t} \tag{3}$$

and this decaying exponential is a good representation of the frictional decay in each case.

Relevance to modelling friction

The results of this experimental study suggest that a critical slip displacement is not a valid assumption for sea ice. It is therefore unlikely that the same rate and state models used for rock friction will be useful for sea ice friction. However, the principles behind such a model still apply: log-linear rate dependence of friction has been shown to be a useful simplification (Lishman et al., 2009; Fortt and Schulson, 2009), and memory effects have been shown to be important (Lishman et al., 2011, as well as the current work). It therefore seems worth pursuing a new model of state dependence which allows for a critical slip time rather than a critical slip displacement. One simple way to do this is to replace the (-V/L) term in equation 1b with a term ($-1/t_c$), which maintains dimensional consistency. Doing this, we get a new rate and state law:

$$\mu = \mu_0 + \theta + A \ln \frac{V}{V^*} \tag{4a}$$

$$\frac{d\theta}{dt} = -\frac{1}{t_c} \left(\theta + B \ln \frac{V}{V^*}\right) \tag{4b}$$

We can then test this new law against both the previous, displacement-focussed rate and state law, and experimental results for friction under dynamic sliding conditions. Lishman et al., 2011, present data from such a dynamic sliding experiment conducted in the laboratory at -10^{o}C using the experimental configuration of figure 2 and the slip rate profile shown in figure 4a. Here we repeat this experimental data in figure 4b, showing alongside it the predictions of both the standard rate and state model (equation 1) and the new critical time dependent rate and state model (equation 3). In both cases μ_0=0.872, and the rate-dependence term B-A = 0.072 (see Lishman et al., 2011, for the origin of these parameters). V^* is a characteristic velocity for dimensional consistency: we use V^* = 10^{-5}ms^{-1}, as in Lishman et al., 2011. For the original model L=0.2mm (experimentally measured) and A=0.31 (fitted). For the new model, ($1/t_c$) must match the coefficient of exponential decay of equation 3, and so t_c=3s (to 1 significant figure, for simplicity). We find A = 0.05 matches experimental data well with the new model (this value leads to instability in the original model). In figure 4b we see clearly that the assumption of a critical slip displacement is flawed, and that with the assumption of a critical slip time the limited friction decay on deceleration (at ~8mm on fig 4b), the two stage frictional increase during acceleration and steady state sliding (~8-10mm), the rounded frictional peak (~10mm) and the long (~10s) frictional decay under steady state sliding (~10-20mm) are all best modelled by the new rate and state equations. We therefore conclude that sea ice friction is best modelled as having a critical slip time, and that the standard rate and state equations, adapted to reflect this, accurately model dynamic sea ice friction.

We also note two important caveats. Firstly, the memory effects encapsulated by equation 3 are necessarily restricted to incorporate the events of the previous 10s or so. For dynamic sliding in the various scales investigated here, this seems to be a useful model. However, we know that at zero slip rate (and by continuity at very low slip rates) consolidation occurs, and that this process has a memory much greater than 10s (i.e. events over 10s in the past can still affect the present). A complete model of sea ice friction would therefore require a second state variable, which would account for these low-slip-rate friction healing effects. This model would also make some intuitive sense, with one catch-all state term covering lubrication effects at non-zero slip rates, and another state term covering consolidation effects at slip rates very close to zero.

Secondly, we note from Fortt and Schulson, 2009, that the assumption of velocity-weakening (that is, decreasing friction with increasing slip rate) is only valid for slip rates above about $10^{-5}ms^{-1}$, and below this value our proposed model is no longer valid.

A further caveat is that the parameterisation used in this study will be dependent on environmental conditions. In particular, we believe that temperature will affect frictional memory, although that hypothesis is not supported by this study (perhaps because our temperature range is small compared to the absolute melting point of ice). One intriguing possibility is that the findings of this study may be relevant to crystalline materials other than ice, provided those materials are at a homologous temperature (in this case $T \approx 0.96\ T_m$). Rice (2006) observes that earthquake dynamics are controlled by extremely narrow shear zones, in which significant thermal weakening occurs and the rock may indeed be at a homologous temperature to the sea ice studied in the present work. It is somewhat difficult to run laboratory rock friction experiments at temperatures close to melting: however, it is much easier to run laboratory ice friction experiments at very low temperatures well away from the melting point ($T \approx 0.8\ T_m$, or around -50^oC) and this seems a promising route for further research along the lines of the present study.

Conclusions

The critical slip of sea ice (at temperatures close to melting) has been assumed to be over a fixed displacement but actually occurs over a fixed time. The experiments outlined in this study have shown that this critical slip time remains constant over a range of slip rates. A simple rule of thumb for engineering purposes is that memory effects in ice friction decay by a factor of 1/*e* over 3s, and are negligible beyond 10s. This understanding can then be used to adjust a standard first order rate and state friction model, and this new model provides an excellent prediction of dynamic friction. The model has the further advantage of computational simplicity, and provides an empirical bridge between Amonton's law and more detailed physical explanations of the micromechanical controls on ice friction. A second order rate and state model might also be able to incorporate the effects of healing at very low slip rates. Further work may answer the question of whether the friction behaviour described in this work is a quirk of columnar sea ice, or whether it may apply more generally to crystalline materials close to their melting temperature.

Acknowledgments

This work was funded by the National Environmental Research Council. The ice tank work was supported by the European Community's Sixth Framework Programme through the grant to the budget of the Integrated Infrastructure Initiative HYDRALAB III, contract 022441(RII3). The authors would like to thank the Hamburg Ship Model Basin (HSVA), especially the ice tank crew, for the hospitality and technical and scientific support. D.F. would like to thank the Leverhulme Trust for the award of a prize that made his participation in the HSVA experiments possible. The authors would like to thank Steve Boon, Eleanor Bailey, Adrian Turner, and Alex Wilchinsky for their contributions to the ice tank work.

References

Fortt, A.L., and Schulson, E.M., 2009. Velocity-dependent friction on Coulombic shear faults in ice. Acta Materiala, 57, 4382-4390.

Hatton, D.C., Sammonds, P.R., and Feltham, D.L., 2009. Ice Internal Friction: Standard Theoretical Perspectives on Friction Codified, Adapted for the Unusual Rheology of Ice, and Unified. Philosophical Magazine, 89:31, 2771-2799.

Lishman, B., Sammonds, P.R., Feltham, D.L., and Wilchinsky, A., 2009. The Rate- and State-Dependence of Sea Ice Friction. In proceedings of Port and Ocean Engineering under Arctic Conditions, 2009.

Lishman, B., Sammonds, P.R., and Feltham, D.L., 2011. A rate and state friction law for saline ice, J. Geophys. Res., 116, C05011, doi:10.1029/2010JC006334.

Maeno, N., and Arakawa, M., 2004. Adhesion Shear Theory of Ice Friction at Low Sliding Velocities, Combined with Ice Sintering. Journal of Applied Physics, 95, 134-139.

Oksanen, P., and Keinonen., J., 1982. The Mechanism of Friction of Ice. Wear, 78, 315-324.

Rice, J. R. (2006). Heating and weakening of faults during earthquake slip. J. Geophys. Res., 111, B05311.

Ruina, A. (1983). Slip instability and state variable friction laws. J. Geophys. Res., 88, 10359-10370.

Location	Laboratory	Ice tank
Ice thickness (m)	0.1	0.25
Water salinity (ppt)	33	33
Bulk ice salinity (ppt)	10.8	7.3
Ice density (kg m^{-3})	930	931

Table 1: Experimental ice details

Experiment Number	Location	Temp. / ^{o}C	Slip Rate V_2/ mms^{-1}	Hold Time / s	Normal Load / N	μ_2^{ss}	μ_{peak}
1	UCL	-10	0.1	100	500	0.82	1.37
2	UCL	-10	0.1	100	1000	0.85	1.35
3	UCL	-2	0.1	100	500	0.69	1.07
4	UCL	-2	0.1	10	500	0.73	0.99
5	UCL	-10	1	100	500	0.60	1.01
6	UCL	-10	1	100	500	0.57	1.14
7	UCL	-10	1	100	1000	0.60	1.18
8	UCL	-10	1	10	500	0.87	1.10
9	UCL	-10	1	1000	500	0.59	1.28
10	UCL	-2	1	100	500	0.40	0.84
11	UCL	-2	1	10	500	0.25	0.51
12	UCL	-2	1	1000	500	0.24	0.76
13	HSVA	-10	16	100	600	0.39	0.78
14	HSVA	-10	16	100	600	0.47	1.12

Table 2. Experimental configurations.

Figure Captions

Figure 1. Idealised evolution of friction μ as a function of slip displacement, for constant normal load, under an instantaneous increase in slip rate (after Ruina, 1983.) The dash-dotted box shows the region in which our later experiments are plotted.

Figure 2. Schematic of experimental apparatus. The ice blocks are milled to dimensions 300 × 100 × 100mm. The entire apparatus shown is housed in a temperature-controlled environmental chamber. The actuator is controlled hydraulically. The x-y plane facing us is the upper surface of the ice.

Figure 3a. Slip rate profile, as a function of time, for an experiment with $V_1 = 0$ and $V_2 = 1mms^{-1}$. The solid line shows the programmed actuator speed, while the markers show the measured actuator speed. The actuator acceleration is around $1mms^{-2}$ in the laboratory experiments.

Figure 3b. Time evolution of friction for experiments 1-4 (see table 2) with $V_1 = 0$ and $V_2 = 0.1mms^{-1}$.

Figure 3c. Time evolution of friction for experiments 5-12 (see table 2) with $V_1 = 0$ and $V_2 = 1mms^{-1}$.

Figure 3d. Time evolution of friction for experiments 13 and 14 (see table 2) with $V_1 = 0$ and $V_2 = 16mms^{-1}$.

Figure 4a. Slip rate profile, as a function of time, for dynamic sliding experiments. The diamond markers show the measured slip rate during the experiment, while the solid line shows the linear approximation used to model the profile.

Figure 4b. Comparison of the predicted friction under the standard rate and state model (grey, short-dashed line) and the new critical time dependent model (black, long dashed line) to experimental measurements. The measurements shown are from a laboratory experiment at -10°C, over the varying slip profile shown in figure 4a.

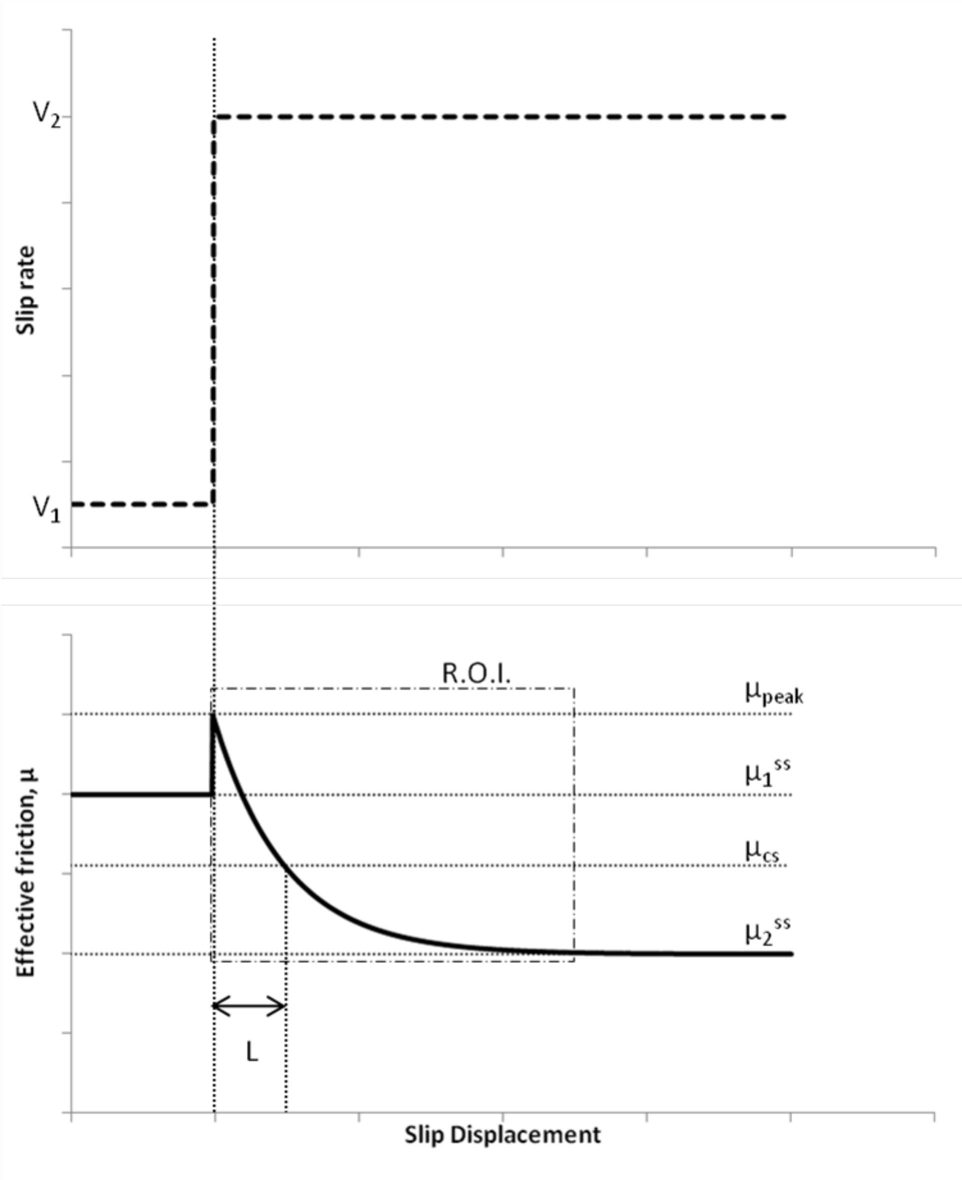

V$_2$
V$_1$
Slip rate
R.O.I.
μ_{peak}
μ_1^{ss}
μ_{cs}
μ_2^{ss}
Effective friction, μ
L
Slip Displacement

FIGURE 1

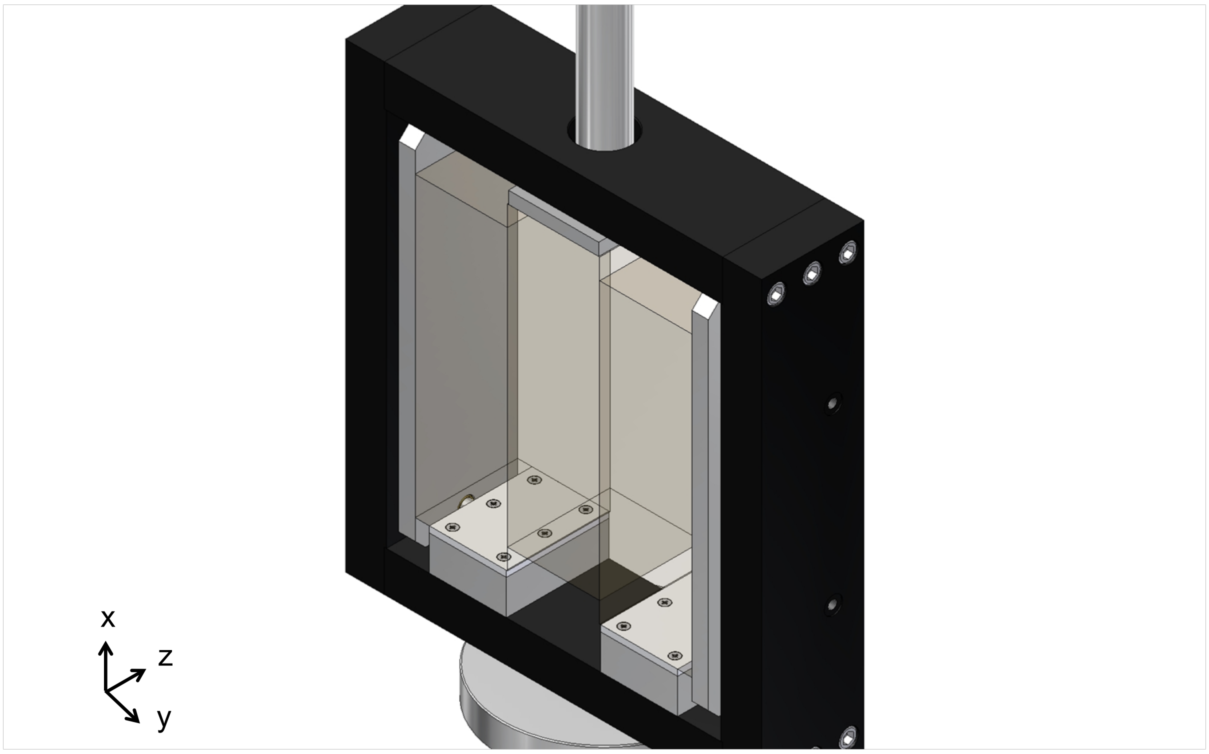

FIGURE 2

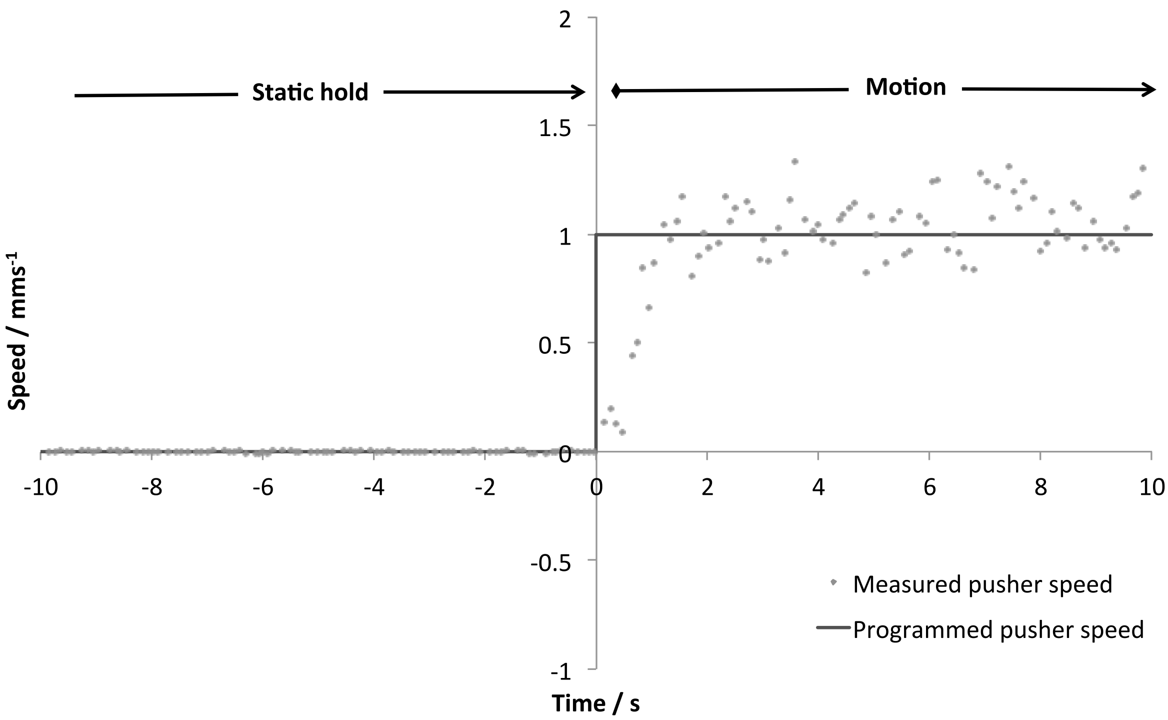

Static hold
Motion
Speed / mms-1
Time / s
Measured pusher speed
Programmed pusher speed

FIGURE 3a

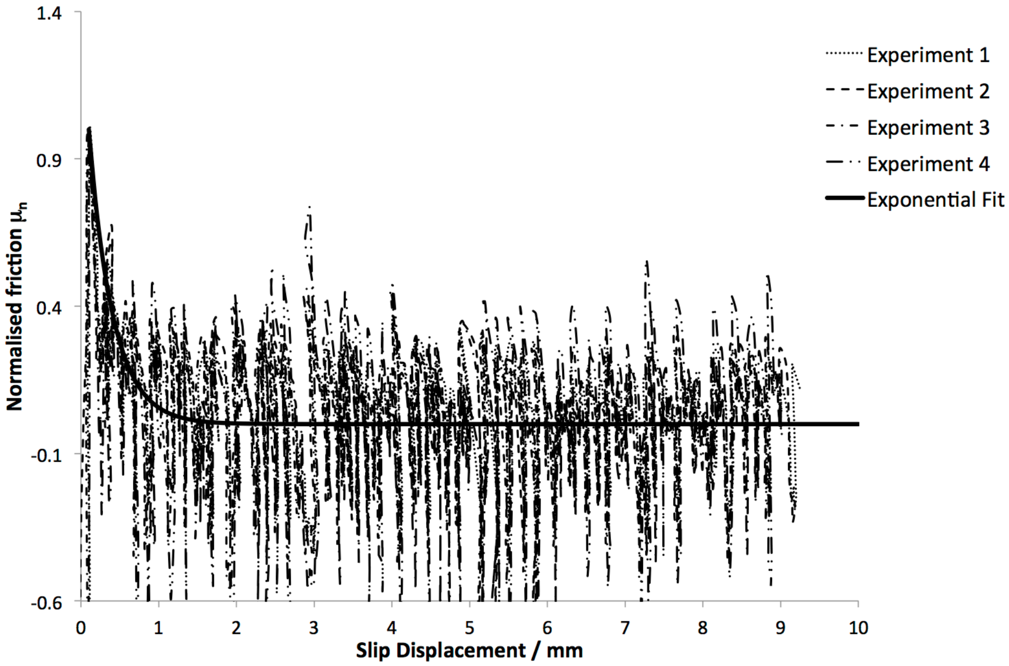
1.4
0.9
0.4
-0.1
-0.6
0
1
2
3
4
5
6
7
8
9
10
Normalised friction μn
Slip Displacement / mm
Experiment 1
Experiment 2
Experiment 3
Experiment 4
Exponential Fit

FIGURE 3B

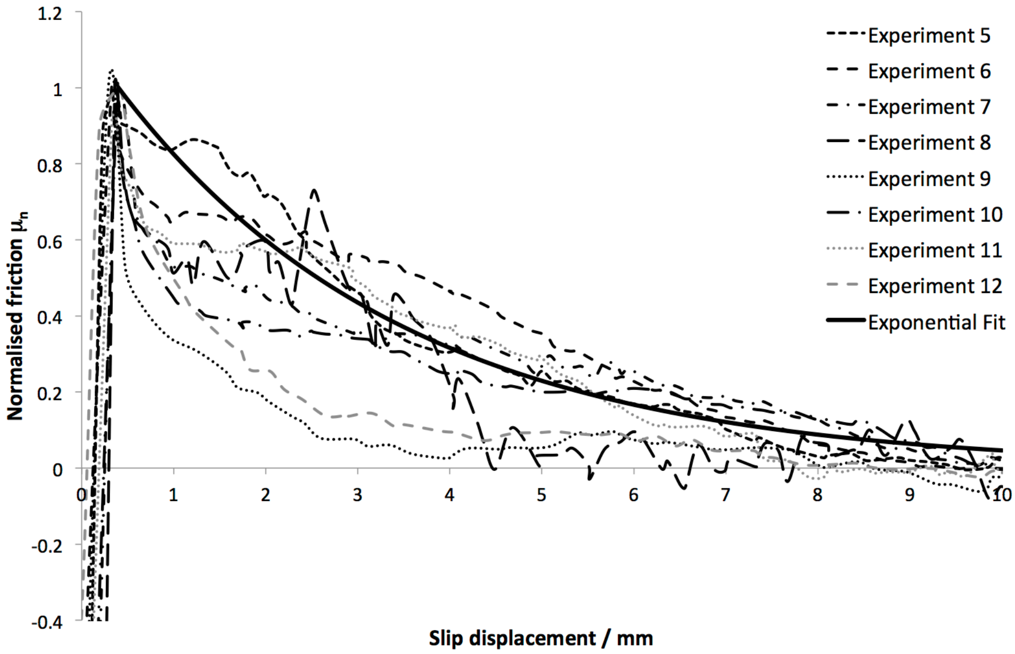
Normalised friction μn
Slip displacement / mm
1.2
1
0.8
0.6
0.4
0.2
0
-0.2
-0.4
0
1
2
3
4
5
6
7
8
9
10
Experiment 5
Experiment 6
Experiment 7
Experiment 8
Experiment 9
Experiment 10
Experiment 11
Experiment 12
Exponential Fit

FIGURE 3C

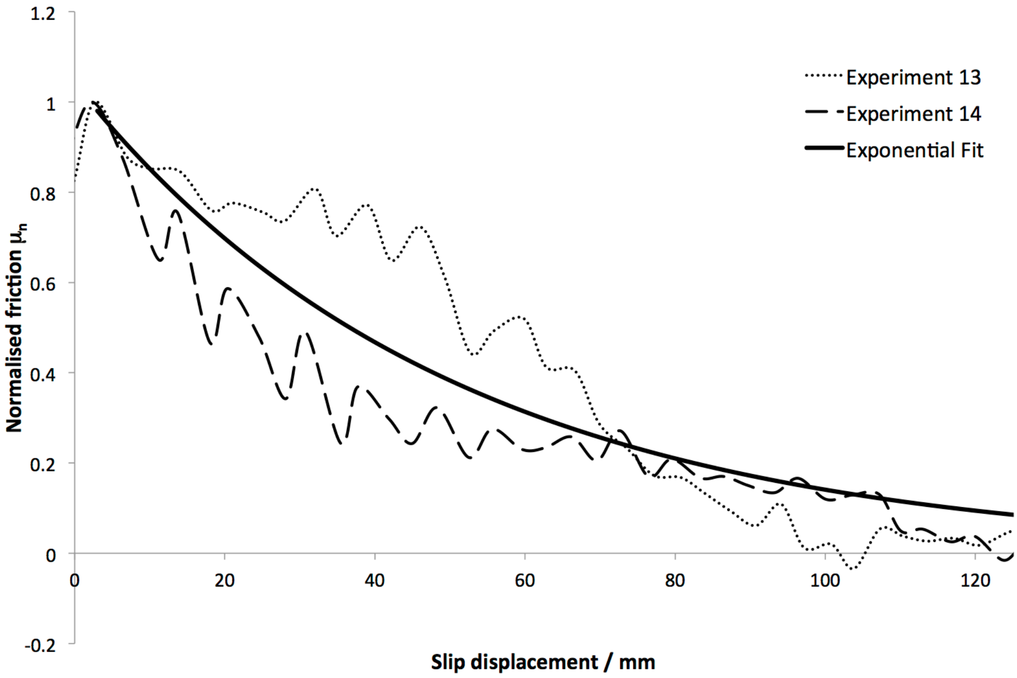

297
298 FIGURE 3D
299

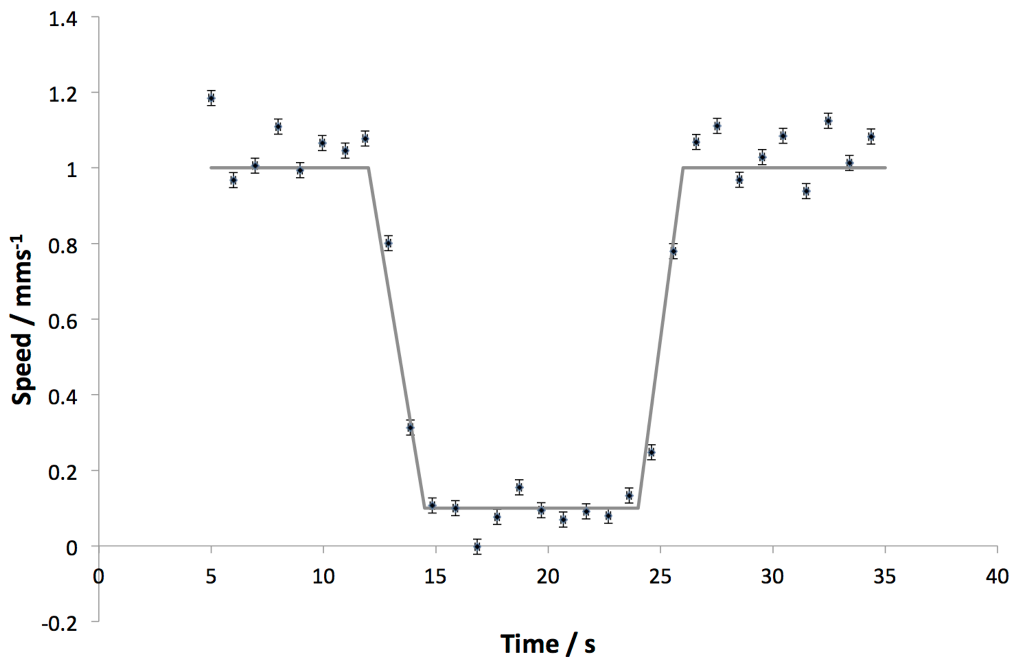

FIGURE 4A

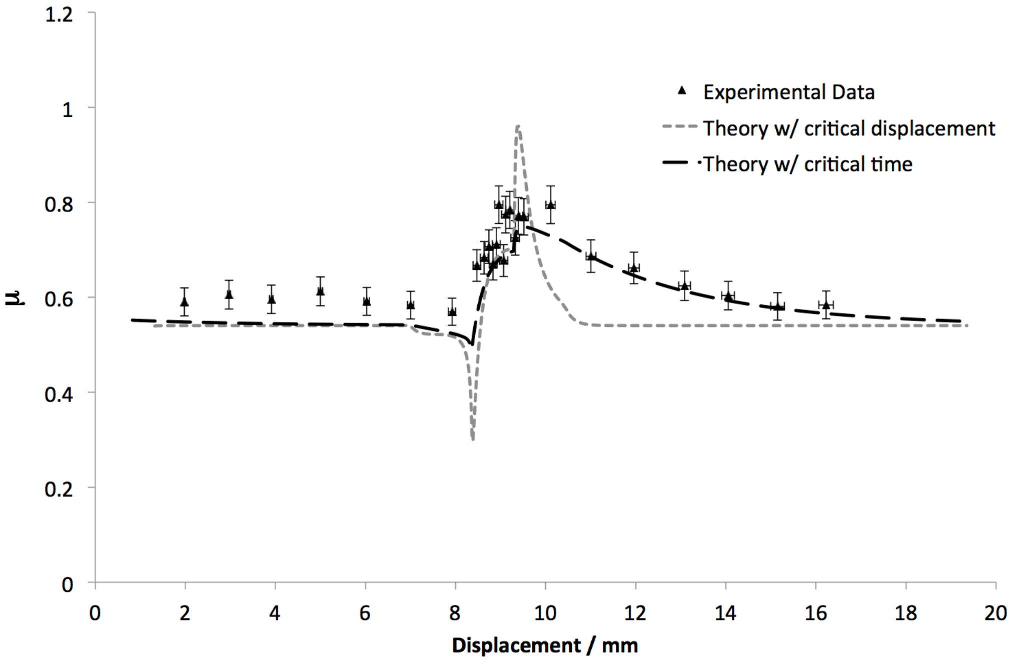

Experimental Data
Theory w/ critical displacement
Theory w/ critical time
μ
Displacement / mm
1.2
1
0.8
0.6
0.4
0.2
0
2
4
6
8
10
12
14
16
18
20

FIGURE 4B